Imaging the Electrostatic Potential of Transmembrane Channels: Atomic Probe Microscopy of OmpF Porin

Ansgar Philippsen,* Wonpil Im,† Andreas Engel,‡ Tilman Schirmer,* Benoit Roux,† and Daniel J. Müller§

*Structural Biology, Biozentrum, University of Basel, CH-4056 Basel, Switzerland; †Department of Biochemistry, Weill Medical College, Cornell University, New York, New York 10021 USA; ‡M. E. Müller Institute, Biozentrum, University of Basel, CH-4056 Basel, Switzerland; and §Max-Planck-Institute of Molecular Cell Biology and Genetics, D-01307 Dresden, Germany

ABSTRACT The atomic force microscope (AFM) was used to image native OmpF porin and to detect the electrostatic potential generated by the protein. To this end the OmpF porin trimers from *Escherichia coli* was reproducibly imaged at a lateral resolution of ~0.5 nm and a vertical resolution of ~0.1 nm at variable electrolyte concentrations of the buffer solution. At low electrolyte concentrations the charged AFM probe not only contoured structural details of the membrane protein surface but also interacted with local electrostatic potentials. Differences measured between topographs recorded at variable ionic strength allowed mapping of the electrostatic potential of OmpF porin. The potential map acquired by AFM showed qualitative agreement with continuum electrostatic calculations based on the atomic OmpF porin embedded in a lipid bilayer at the same electrolyte concentrations. Numerical simulations of the experimental conditions showed the measurements to be reproduced quantitatively when the AFM probe was included in the calculations. This method opens a novel avenue to determine the electrostatic potential of native protein surfaces at a lateral resolution better than 1 nm and a vertical resolution of ~0.1 nm.

INTRODUCTION

Local electrostatic properties play a central role in a variety of biological processes. A detailed characterization of the structure and function of biological systems requires an understanding of the strength and location of their electrostatic interactions (Honig and Nicholls, 1995; McLaughlin, 1989; Nakamara, 1996; Sharp and Honig, 1990). Transmembrane channels require ion selectivity to maintain the electrostatic gradient across a cell membrane. Theoretical calculations predicted (Im et al., 2000; Roux and MacKinnon, 1999) that this selectivity is likely to involve electrostatic potentials established within the protein structure (Roux et al., 2000; Schirmer and Phale, 1999). However, direct measurements of the electrostatic properties of proteins at a sufficient spatial resolution allowing the comparison with theoretical calculations have not been available yet.

The atomic force microscope (AFM) (Binnig et al., 1986) allows surfaces of biological samples to be imaged in liquids (Drake et al., 1989). As demonstrated on various native protein assemblies, the resolution of AFM topographs can be better than 1 nm enabling substructures of individual proteins to be identified (Czajkowsky et al., 1999; Engel and Müller, 2000). Because single proteins can exhibit individual structural deviations, common structural features among similar proteins are obtained by averaging techniques (Müller et al., 1998; Schabert and Engel, 1994). Standard deviation (SD) maps of averaged topographs show enhanced values at variable protein domains, allowing their identification. The conformations of such variable substructures can be further unraveled by the classification of AFM topographs (Engel and Müller, 2000; Müller et al., 1998).

The AFM probe can also be used as a sensor to probe charges of biological surfaces immersed in buffer solution (Butt et al., 1995). Here, the electrostatic double-layer (EDL) force (Israelachvili, 1991) interacting between the charged probe and charged regions of the biological sample can contribute significantly to the AFM topograph recorded (Müller and Engel, 1997; Rotsch and Radmacher, 1997) and can be tuned by the electrolyte concentration and the pH of the buffer solution. The DLVO theory describes the exponential decay of the EDL force as a function of the surface separation (Israelachvili, 1991). Whereas AFM probes have been used to measure the average surface charges from force-separation curves (Butt, 1991; Ducker et al., 1991), surface charge maps have been obtained at 40-nm lateral resolution by recording force-separation curves at each pixel of the sampled surface (Heinz and Hoh, 1999; Rotsch and Radmacher, 1997).

In this work we used AFM to image transmembrane channels of native proteins and to map their electrostatic potential. To this end, high-resolution AFM topographs of OmpF porin were recorded under variable electrostatic conditions, and the electrostatic potential of the protein channel was decomposed by subtracting topographs recorded at different electrostatic contributions. As an example we have chosen the transmembrane channel-forming protein OmpF porin located in the outer membrane of *Escherichia coli*. OmpF porin exists as stable trimeric structures, and the 340-amino acids-long polypeptide of the OmpF monomer is

Submitted September 14, 2001, and accepted for publication November 14, 2001.

Address reprint requests to Daniel J. Müller, PhD, Max-Planck-Institute of Molecular Cell Biology and Genetics, Pfotenhauerstr. 108, D-01307 Dresden, Germany. Tel.: 49-351-210-2586; Fax: 49-351-210-2020; E-mail: mueller@mpi-cbg.de.

0006-3495/02/03/1667/10 $2.00

folded into 16 antiparallel β-strands that form a large hollow transmembrane β-barrel structure (Cowan et al., 1992). An infolding loop forms the eyelet of each barrel constricting the passage of ions and of hydrophilic solutes up to an exclusion size of ~600 kDa (Nikaido and Saier, 1992; Schirmer, 1998). Translocation rate of the pore and solute concentration gradient across the membrane show a linear relation. The ion selectivity of the pore, however, increases with decreasing electrolyte concentration (Schirmer and Phale, 1999). This selectivity is altered by modification of the charged amino acids of the pore lining (Saint et al., 1996a), which are thought to produce a characteristic electric field at the pore constriction (Cowan et al., 1992; Weiss et al., 1991). Hence, it has been suggested that the charges of the porin constriction primarily modulate the pore selectivity (Klebba and Newton, 1998; Schirmer, 1998). However, the electrostatic potential at the entrance of the OmpF porin channel was not explored in these calculations.

MATERIALS AND METHODS

Sample preparation

OmpF porin trimers from *E. coli* strain BZ1110/PMY222 (Hoenger et al., 1993) were purified and reconstituted in presence of dimyristoyl phosphatidylcholine and lipopolysaccharides as described (Hoenger et al., 1990). The protein crystals were adsorbed to freshly cleaved mica (Müller et al., 1997), and the sample was mounted on the piezoelectric scanner of the AFM (Nanoscope III, Digital Instruments, Santa Barbara, CA) equipped with a liquid cell. Cantilevers used had nominal force constants of 0.09 or 0.02 N/m and oxide-sharpened Si_3N_4 probes (Olympus Ltd., Tokyo, Japan). The piezoelectric scanner of the AFM (scan range of $100 \times 100\ \mu m^2$) was calibrated (Müller and Engel, 1997).

AFM imaging

All topographs were recorded using the constant force mode as described (Müller et al., 1999). We investigated only double-layered OmpF porin membranes, facing both extracellular surfaces toward each other. Thus, the periplasmic porin surface imaged by AFM was separated to the supporting mica surface by an intermediate porin layer (Schabert et al., 1995). These sandwiched protein layers minimized possible electrostatic influences of the support. It may be considered that the surface charge density of mica (-0.0025 C/m^2) (Pashley, 1981) is ~24 times smaller than that detected on the periplasmic porin surface (-0.06 C/m^2) (Müller and Engel, 1997).

At KCl concentrations $\leq$300 mM EDL forces (Israelachvili, 1991) contribute to repulsive interactions between Si_3N_4 probe and periplasmic OmpF porin surface (Müller and Engel, 1997; Müller et al., 1999). Decreasing of the electrolyte concentration resulted in an increased EDL repulsion (Müller and Engel, 1997). In this case, submolecular resolution was only obtained after enhancing the applied force carefully until protein substructures became visible. Because of the EDL interaction compensated most of the applied force, the net force interacting between AFM probe and protein was equal to the net force when imaged at 300 mM KCl. A criterion for the minimization of the net force was the protein structure, which was not deformed by the imaging process. In summary, all topographs were recorded at applied forces slightly above ($\Delta F = 25$ pN) those of the EDL repulsion. Fine-tuning of the applied force was adjusted comparing the height profiles acquired simultaneously in trace and retrace direction until the deformation of the sample (Weisenhorn et al., 1993) disappeared. Image processing of the raw data was done as previously described (Müller et al., 1998; Schabert and Engel, 1994).

Theoretical considerations

In the constant force mode, the AFM measured displacements represent the relative position of the probe at which the applied external force F_{ext} is exactly counterbalanced by $\langle F_{mol}\rangle$, the time-averaged microscopic molecular forces acting between probe and OmpF, i.e., the displacement of the probe corresponds to the condition $F_{ext} = \langle F_{mol}\rangle$. It can be shown that $\langle F_{mol}\rangle$ can be expressed as the derivative of a reversible work function $G(\mathbf{R}_{tip})$ (Kirkwood 1934)

$$\langle F_{mol}\rangle = -\frac{\partial G(\mathbf{R}_{ip})}{\partial Z_{tip}}$$

in which Z_{tip} is the direction perpendicular to the membrane plane. In fact, $G(\mathbf{R}_{tip})$ corresponds to the free energy of the system with the probe at a fixed position $\mathbf{R}_{tip}$, relative to OmpF porin. This free energy, which includes contributions from the influence of the aqueous solvent and the electric double layer from the electrolyte, as well as various nonpolar interactions, can be written as (Roux and Simonson, 1999)

$$G(\mathbf{R}_{tip}) = G_{np}(\mathbf{R}_{tip}) + G_{elec}(\mathbf{R}_{tip})$$

Because we are mostly concerned with the dependence of the long-range electrostatic contribution, G_{elec}, upon variations of the salt concentration, the nonpolar contribution, G_{np}, which is expected to be short-range, will be ignored in the following. Assuming that the solvent and electrolyte are described according to macroscopic continuum electrostatics, G_{elec} is given by (Madura et al., 1995; Roux and Simonson, 1999)

$$G_{elec} = \frac{1}{2}\sum_i q_i\phi(i)$$

in which q_i is the charge of the i-th atom in the system, and $\phi(i)$ is the electrostatic potential at the position of the i-th atom in the system calculated from the Poisson-Boltzmann (PB) equation (Im and Roux, 1998; Madura et al., 1995)

$$\nabla\cdot(\epsilon(\mathbf{r})\nabla\phi(\mathbf{r})) + \bar{\kappa}^2(\mathbf{r})\phi(\mathbf{r}) = 4\pi\rho(\mathbf{r})$$

in which $\epsilon(\mathbf{r})$ is the space-dependent dielectric constant, $\bar{\kappa}^2(\mathbf{r})$ is the Debye-Hückel ionic screening factor, and $\rho(\mathbf{r})$ is the charge density of the molecular species being considered. All atomic details about OmpF and the AFM probe can be incorporated in the PB equation via the space-dependent functions $\epsilon(\mathbf{r})$, $\bar{\kappa}^2(\mathbf{r})$, and $\rho(\mathbf{r})$.

If it is assumed that the probe interior is exactly the same as the surrounding solution in terms of a dielectric constant and salt concentration (Approach A), the electrostatic forces are given by $F = qE$ in which E represents the electrostatic field generated by OmpF. In a realistic treatment of the physical probe (Approach B), other contributions to the force arising from the low dielectric constant of the probe have to be included.

Electrostatic potential calculation

The electrostatic calculations are based on the atomic structure of OmpF (2OMF) (Cowan et al., 1992). The atomic coordinates were transformed such that the molecular threefold axis of the central trimer coincided with the z axis (with positive z toward the periplasmic side) and the center of the molecule was at the origin. The protein charges were set according to the CHARMM parameter set (MacKerell et al., 1998), with the net charges of E296 and D312 set to zero according to theoretical pKa calculations (Karshikoff et al., 1994). However, the three arginines in the cluster R42, R82, and R132 were treated charged as discussed before (Schirmer and

Phale, 1999). The bulk solution and the membrane were approximated as continuous media (for details see below). Optimized Born radii for proteins were used to setup the solvent-protein dielectric boundary (Nina et al., 1997). A Debye-Hückel screening factor corresponding to 300, 100, or 50 mM salt concentrations was assigned to the ion-accessible region.

Approach A

Seven OmpF trimers were embedded into a membrane bilayer and arranged according to the rectangular lattice (P2, a = 7.6 nm, b = 13.5 nm) of the two-dimensional OmpF crystals investigated experimentally. The sidechains of K10, E183, and K305 at the periplasmic side are not defined in the x-ray structure (see also Fig. 2). These residues were structurally included as follows: All stereochemically accessible side-chain conformations were generated by systematic variation of their side-chain dihedrals. From this ensemble, the mean position of the side-chain amino group or the two carboxyl oxygens were determined. The three residues were truncated to alanine, and a point charge was placed at the appropriate mean position.

The linearized PB equation was solved using UHBD (Madura et al., 1995) on a 281 × 281 × 101 grid with a 0.1-nm grid spacing. Externally generated dielectric constant (epsilon) grids were used: An epsilon of 4 was assigned to grid positions within the protein (distance of the nearest protein atom < (protein atom radius + 0.15 nm)/2). The membrane was modeled by assigning $\epsilon = 40$ to the presumed position of the lipid head-groups (-1.4 nm $< z < -0.4$ nm and 1.4 nm $< z <$ 1.9 nm) and an $\epsilon = 2$ to the membrane core. The dielectric constant of the transmembrane pore and of the surrounding aqueous solution was set to 80. From the calculated electrostatic potential, the force at each grid point was simply calculated following $F = qE$ in which E represents the derivative of the electrostatic potential taken numerically.

The program used to generate the external epsilon grid was developed by A.P. and is available upon request. Data interpretation and visualization (see Figs. 2, 4, and 5) were done using DINO (http://www.dino3d.org). Molecular surfaces were calculated with MSMS (Sanner et al., 1996).

Approach B

The AFM probe was modeled as a sphere of 1-nm radius, whereas the OmpF trimer was represented with all atomic details. A single OmpF trimer with its symmetry axis oriented along the z axis was embedded in a 3.4-nm-thick ion-impermeable planar membrane. A dielectric constant of 80 was assumed for the bulk solvent region including the aqueous pore region of OmpF, whereas a dielectric constant of 2 was used for the interior of the protein and membrane regions as well as the interior of the AFM probe. An ion exclusion Stern layer of 0.18 nm was used to set the spatial dependence of the ionic screening factor. For each position of the probe, the electrostatic energy was first calculated by solving the PB equation with a coarse grid (101 × 101 × 181 grid with a spacing of 0.1 nm) centered on the OmpF trimer. Periodic boundary conditions were imposed in the direction of the membrane plane. The result of the coarse calculation was then used to set the boundary conditions on the edge of a smaller box to perform a second calculation using a finer grid (with a spacing of 0.05 nm) centered on the periplasmic side of OmpF. Finally, the electrostatic forces were calculated by taking the first derivatives of G_{elec} numerically. All calculations were performed using the PBEQ module in CHARMM.

RESULTS

AFM topographs recorded at different electrolyte concentrations

In previous studies of two-dimensional OmpF porin crystals we have optimized the conditions to image the porin surfaces at subnanometer resolution by AFM (Müller et al., 1999). Topographs of the periplasmic OmpF porin surface recorded in 300 mM KCl, pH 7.8, 10 mM Tris-HCl revealed trimeric domains that protruded by 0.6 ± 0.1 nm ($n = 92$) from the lipid bilayer surface (Fig. 1 *A*). At a force of ~25 pN applied between AFM probe and protein (see Materials and Methods) each trimer compromises a tripartite protrusion and three transmembrane channels that are separated by 1.2-nm-thick walls. The outlined circle and ellipse surround individual polypeptide loops between 2 and 5 amino acids size, each loop connecting two antiparallel β-strands lining the transmembrane pore. Correlation averaging of the porin trimer enhanced common structural details among individual trimers (Fig. 1 *B*) but blurred variable areas of their subdomains (compare with trimers shown in raw data, Fig. 1 *A*). Nevertheless, the characteristic shape of the averaged transmembrane channel appeared more pronounced showing an elliptical cross-section of a = 3.4 nm and b = 2.0 nm. Comparison with the SD map (Fig. 1 *C*) allows direct assignment of variable structural regions of the native protein (Fig. 1 *D*) (Müller et al., 1998).

Fig. 1, *E* and *H* show the periplasmic surface of the same OmpF crystal as imaged in Fig. 1 *A* but recorded after the electrolyte concentration of the buffer solution (pH 7.8, 10 mM Tris-HCl) has been decreased from 300 to 100 mM KCl (Fig. 1 *E*) and to 50 mM KCl (Fig. 1 *H*). Similar to the topograph recorded under 300 mM KCl (Fig. 1 *A*) the tripartite protrusions surrounding the trimeric center were clearly visible and extended by 0.6 ± 0.1 nm from the bilayer surface. Again, correlation averaging enhanced the common structural details of the trimers (Fig. 1, *F* and *I*) and the SD maps (Fig. 1, *G* and *J*) allowed structural areas of enhanced variability to be assigned. As expected, the structural variability of OmpF remained mainly unaffected by the electrolyte concentrations (Fig. 1, *C*, *G*, and *J*).

Comparison of AFM topographs and atomic structure

As visible from the topographs (Fig. 1), single OmpF porins were imaged at a sufficient resolution to visualize short polypeptide β-turns connecting transmembrane β-strands. To reveal the accuracy of the porin trimer recorded at 300 mM KCl, we superimposed its correlation average and SD map with the atomic porin model in three dimensions (Fig. 2). The AFM topography shows excellent agreement to structural data from x-ray crystallography (Schabert et al., 1995). Interestingly, the SD map of the porin surface (blue shaded in lower right pore) exhibited enhanced values (variability) close to residue K305, which is found disordered in the x-ray structure. The other two disordered sidechains at the periplasmic surface (K10 and E183) were not observed in the SD map. These two residues may not have been sensed by the AFM probe, because they do not reach the topographic surface. This agreement of structure and vari-

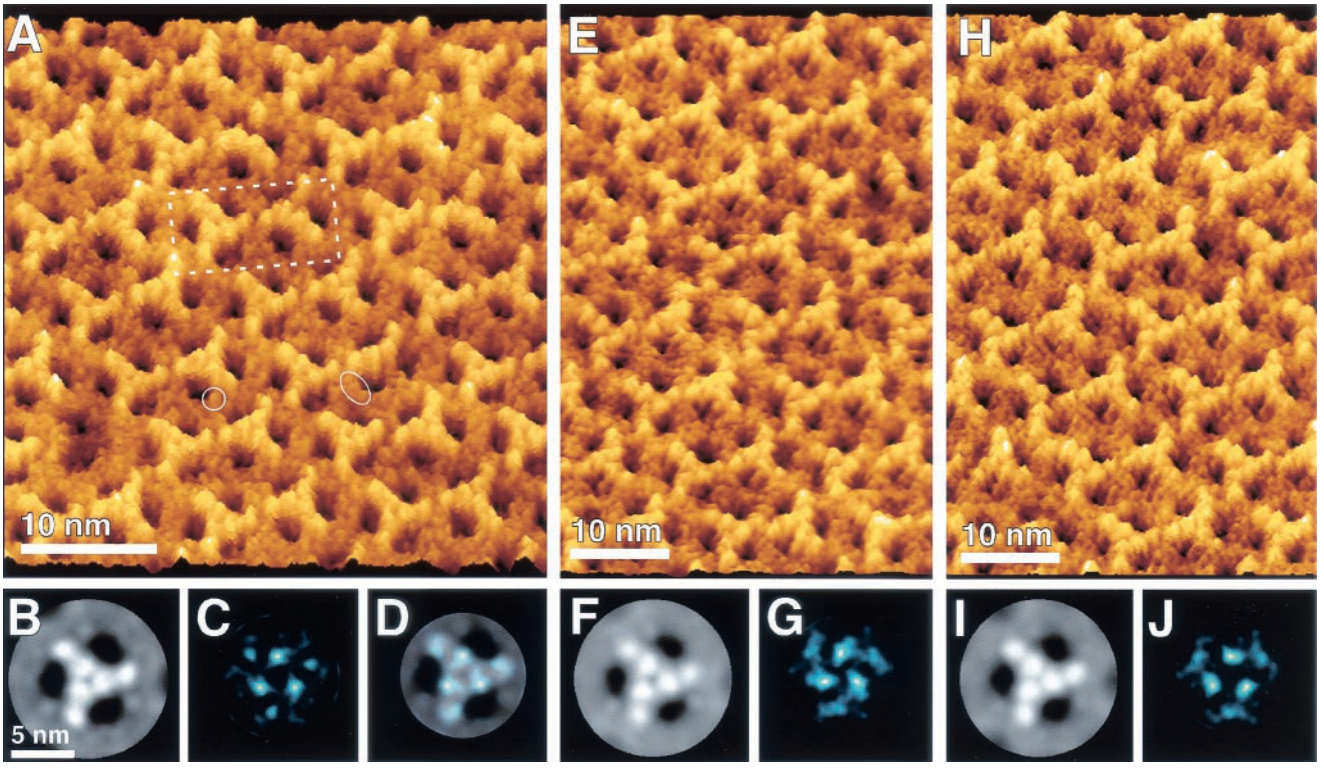

FIGURE 1 Periplasmic surface of OmpF porin recorded in buffer solution (pH 7.8, 10 mM Tris-HCl) at different electrolyte concentrations. (A) AFM topograph as revealed in 300 mK KCl. Single porin trimers forming rectangular unit cells (a = 13.5 nm, b = 8.2 nm as outlined) of the two-dimensional crystal were clearly visible. Circle and ellipse indicate short β-strand-connecting turns observed on individual porin monomers (comp. Fig. 2). The topograph was recorded at a scan frequency of 8 Hz. (*B*) Three-fold symmetrized correlation averaged porin trimer (n = 247) revealed from (*A*). (*C*) The standard deviation (SD) map of (*B*) had a vertical range from 0.05 to 0.23 nm. (*D*) To assess variable structural regions, average and SD maps were superimposed. (*E*) Topography recorded in 100 mM KCl. (*F*) Three-fold symmetrized correlation averaged porin trimer (n = 217) as revealed from (*E*). (*G*) SD map of (*E*) exhibiting a vertical range from 0.04 to 0.21 nm. (*H*) Topography recorded in 50 mM KCl. (*I*) Three-fold symmetrized correlation averaged porin trimer (n = 309) as revealed from (*H*). (*J*) SD map of (*I*) exhibiting a vertical range from 0.07 to 0.23 nm. All topographs were recorded on the same OmpF crystal with identical imaging parameters except the applied force, which was enhanced to compensate for the electrostatic repulsion (see Materials and Methods). The vertical brightness range of (*A*), (*B*), (*E*), (*F*), (*H*), and (*I*) corresponds to 1.5 nm. (*A*), (*E*) and (*H*) were displayed in perspective view.

ability of the porin surface determined by both structural methods is remarkable, considering that the information was obtained under different conditions (i.e., detergent versus lipid membrane, three-dimensional stacking of porin surfaces versus porin surfaces exposed to buffer solution).

Visualizing electrostatic contributions of the transmembrane pore

To visualize local electrostatic interactions between AFM probe and the electrostatic field of porin OmpF we calculated difference maps between the averaged topographs recorded under variable electrolyte concentrations (Fig. 1). The difference map (Fig. 3) exhibited pronounced maxima located at the elliptical entrance of the channels. The height differences of these maxima were 0.3 $\pm$ 0.1 nm and 0.5 $\pm$ 0.1 nm for an electrolyte difference of 200 and of 250 mM KCl, respectively. Because we can exclude structural changes of the rigid pore-forming structures we conclude that the topographic differences reflect the change in electrostatic potential with the repulsive force on the AFM probe increasing with decreasing electrolyte concentration.

Simulating the experiment

The electrostatic potential of OmpF and the resulting force acting on the AFM probe were calculated from a numerical solution of the linearized PB equation using two approaches (A and B) that differ markedly in their treatment of the AFM probe. In particular only approach B explicitly incorporates a model of the probe into the solution of the PB equation.

Approach A

Mimicking the crystalline arrangement investigated, the electrostatic potential of seven symmetrically arranged OmpF trimers embedded into a lipid bilayer was calculated

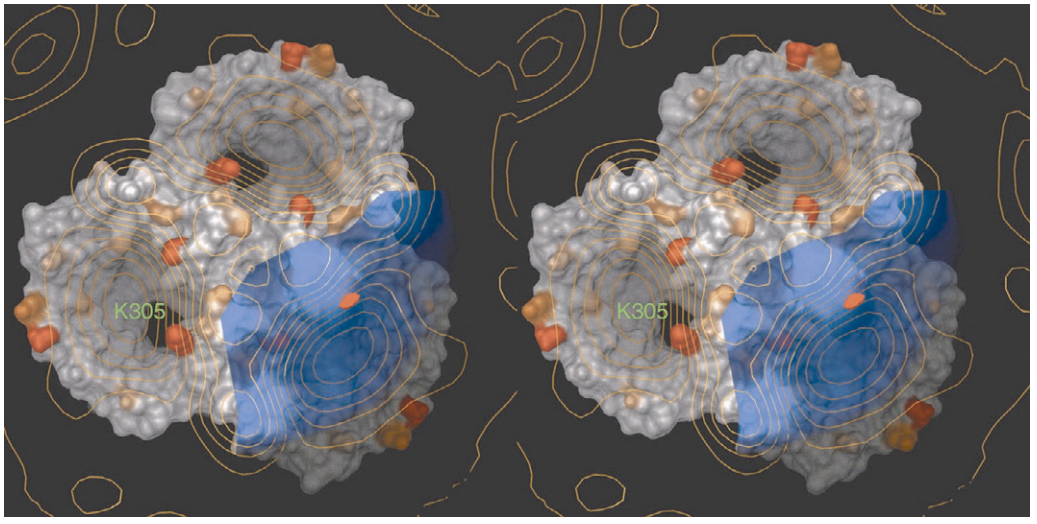

FIGURE 2 Comparing the periplasmic surface of OmpF porin determined by AFM and by x-ray nalysis. The AFM surface (*yellow* contour plot) represents the correlation average calculated from the topograph recorded at 300 mM KCl (Fig. 1 *B*). The underlying molecular surface derived from the crystal structure is color coded according to the crystallographic temperature factors: (*white*) below 60; (*white* to *yellow*) from 60 to 70; (*yellow* to *red*) from 70 to 80; and (*red*) above 80. The three undefined (*red*) sidechains are K10, E183, and K305, of which only K305 is not consistent with the AFM topograph as it protrudes through the topograph and, therefore, directly interacts with the AFM probe. Superimposed onto the lower right pore is the SD map of the correlation average (Fig. 1 *C*) with blue indicating region of height variability

(Schirmer and Phale, 1999). From the resulting potential, the electrostatic force acting on a point charge was calculated for each grid point. The electrostatic potential as well as the *z*-component of the force are displayed in Fig. 4 for 50 and 300 mM monovalent ion concentrations (100 mM ion concentration giving an intermediate result is not shown). As expected, at high salt concentration the electrostatic potential is effectively shielded by the electrolyte. At low salt concentration, the predominantly negative potential extends asymmetrically into the periplasmic space: It is prominent at the outer rim of the transmembrane pore and decreases toward the pore center exhibiting a small positive contribution above the central ridge. Because theoretical calculations published before have mainly focused on the potential inside the channel (Dutzler et al., 1999; Schirmer and Phale, 1999), this phenomenon was not found previously. The isoforce surfaces are contoured at two values: The isosurface at −25 pN represents the approximate force applied during the constant force AFM mode, but cannot explain the observed height difference of 0.5 nm. The isosurface at −5 pN represents the value necessary for a 0.5-nm height difference between the two isosurfaces.

Approach B

Here, the AFM probe was modeled explicitly as a low-dielectric sphere of 1-nm radius. The PB equation was solved for every given position of the probe to calculate the free energy of the system and the resulting force derived numerically (Fig. 5). Two positions of the probe were considered for illustrative purposes: the region with the largest displacement near the center of the aqueous pore (Fig. 5 *B*) and a region with small displacement at the center of the trimer (Fig. 5 *A*). An external applied force of ~25 pN was assumed. It is observed that the average microscopic force is counterbalanced at positions changing by ~0.3 and 0.5 nm when the salt concentration is varied respectively from 300 to 100 mM and from 300 to 50 mM.

DISCUSSION

OmpF porin facilitates the diffusion of hydrophilic solutes across the outer membrane of *E. coli*. Determination of the physical factors influencing the transporting behavior of the transmembrane porin pore will provide information essential for understanding of its function. One important aspect of porin is the experimentally observed cation selectivity increasing reciprocally to the ion concentration of the buffer solution (Lou et al., 1996; Saint et al., 1996a,b). Here we have taken a first step by studying the electrolyte-dependent electrostatic potential of OmpF experimentally and correlated the results with calculations based on the x-ray structure.

AFM clearly shows electrostatic potential of the porin pore

The AFM experiments were performed under identical experimental conditions, i.e., the same AFM probe, same membrane, identical pH, and the same force interacting between probe and OmpF porin (see Materials and Meth-

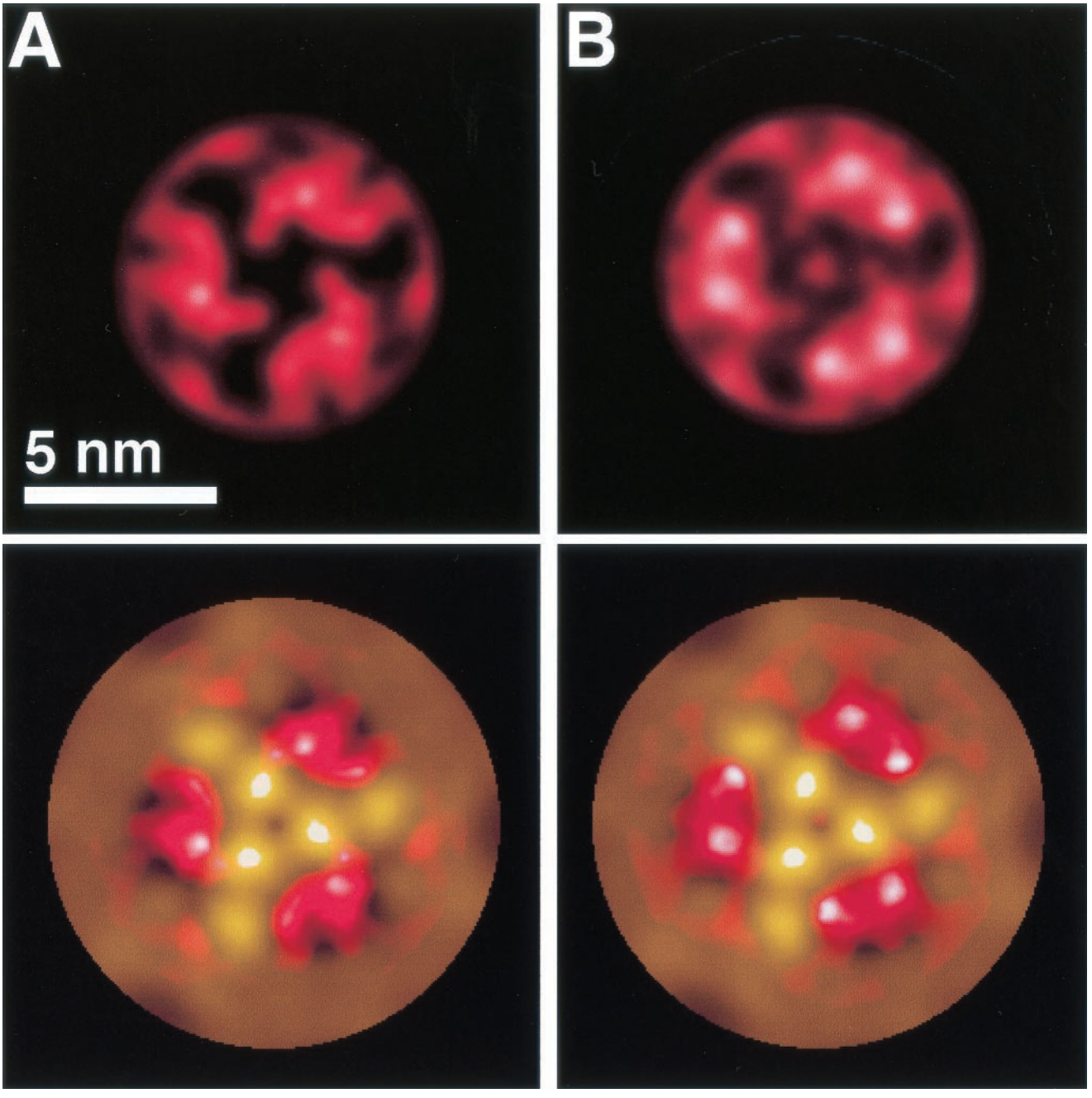

FIGURE 3 Visualizing the electrostatic potential of OmpF porin. Difference maps between topographs recorded of the periplasmic surface at 100 and 300 mM KCl (*A*) and at 50 and 300 mM KCl (*B*). As becomes evident, the main differences between porin trimers recorded at different electrolyte concentrations are located at the entrances of the transmembrane pore. The color scale shaded from white (highest difference) to red (high difference) to black (difference <0.05 nm) corresponds to a vertical height of 0.3 nm (*A*) and of 0.5 nm (*B*). Lower panels show the superimposition of the averaged topograph (colored brown-gold) and the electrostatic potential

ods). The only parameter changed during AFM imaging of the protein surface was the electrolyte concentration itself. As a result of this change an additional repulsive force was observed at the porin pore at low ionic strength. Conformational changes at the periplasmic pore surface can be excluded and repulsion of the negatively charged AFM probe is attributed to a negative electric potential of the pore that is efficiently shielded at higher ionic strength of $\geq$300 mM monovalent electrolyte.

Electrostatic pore potential

The heights of the difference maps are a direct estimate of the electrostatic force between porin and AFM probe. Low-

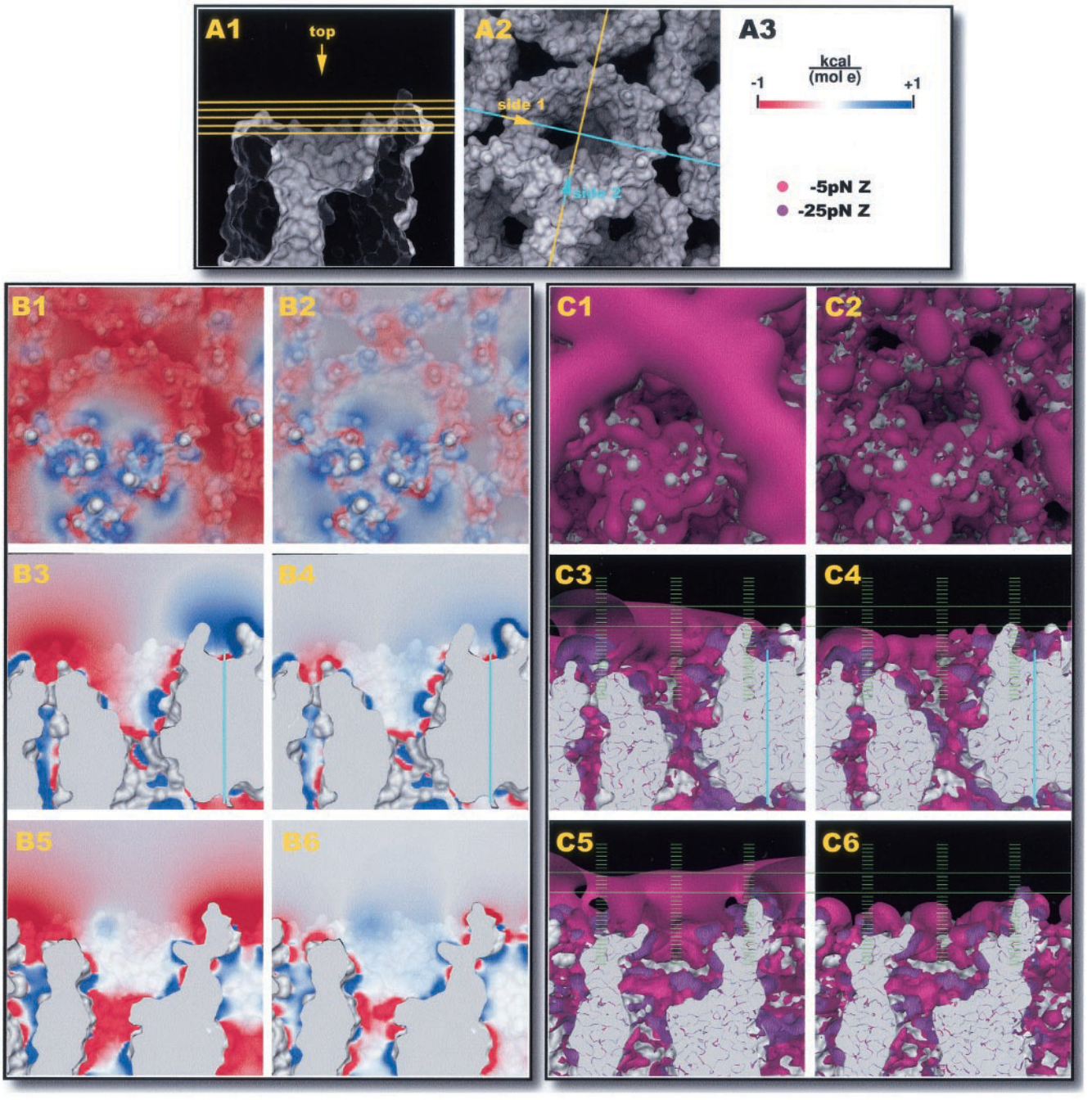

FIGURE 4 Electrostatic potential and force of the OmpF trimer calculated at different electrolyte concentrations. Series (*A*) explains the orientation, viewing direction, slab orientation, and scale used in series (*B*) and (*C*). Three perpendicular views are presented: a top view (*B/C 1/2*) from the periplasmic side onto the OmpF trimer and two side views, one with the trimer axis on the right hand side (*B/C 3/4*, indicated with a cyan line) and one viewing from the axis (*B/C 5/6*). The color coding is explained in (*A3*). Series (*B*) shows the electrostatic potential at 50 mM (*B 1/3/5*) and at 300 mM (*B 2/4/6*) monovalent salt concentration. The topview (*B 1/2*) uses a multilayered transparent slab to convey information within a volume. The slabs in the sideviews (*B 3–6*) are given in (*A2*). The asymmetry of the negative potential extending into the periplasmic space is clearly visible in (*B3*), with a strong contribution on the outer rim of the protein (*left*) and almost no contribution close to the trimer axis (*perpendicular cyan line*). Series (*C*) displays the iso-force surfaces for the *z*-component of the force acting on a 2.51 e unit charge, contoured at −5 pN (*light magenta*) and −25 pN (*dark magenta*), overlayed with a 0.1 nm ruler (*green*). The orientation and ion concentration corresponds to series (*B*), (*C 1/3/5*) are from 50 mM and (*C 2/4/6*) from 300 mM ion concentration. The iso-force surface corresponding to −25 pN cannot explain the measured height difference of 0.5 nm during the AFM experiment, only a lower force iso-surface can do so, at approximately −5 pN (indicated by the two horizontal green lines).

ering the monovalent electrolyte concentration from 300 to 100 mM resulted in a height increase of 0.3 nm at the pore, whereas lowering the electrolyte concentration from 300 to 50 mM resulted in an increase of 0.5 nm. Importantly, the

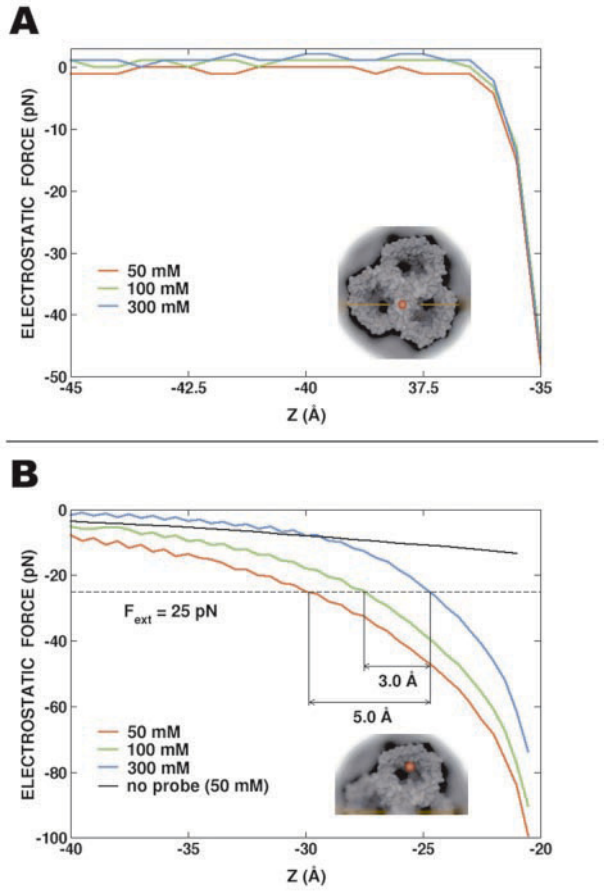

FIGURE 5 Results from numerical solution to the PB equation with explicit presence of the AFM probe. Two approaches of the AFM probe perpendicular to the membrane plane are calculated: (A) along the trimer axis and (B) near the center of the transmembrane pore (see *insets* for positioning of probe). The z vlaue denotes the probe separation from the vertical OmpF center (0 Å), the force is derived from G_{elec}. At a distance of ~36 Å the probe touches the central protrusion of the porin trimer and deforms the molecule (A). (*B*) Aproaching the pore center the probe can travel further detecting the electric potential. The experimentally applied force is indicated with a strippled line. Above the OmpF pore, the average microscopic force is counterbalanced at positions changing by ~3 and 5 Å when the salt concentration is varied from 300 to 100 mM and from 300 to 50 mM, respectively. As a comparison, the gray line indicates the force at 50 mM salt without including the probe into the calculation. The results were calculated using Approach B (see Material and Methods)

SD (Fig. 1) and the electrostatic (Fig. 3) maps exhibited maxima at different locations and, thus, are independent from each other. Assuming a probe radii of ~2 nm, which enables topographs at subnanometer resolution to be achieved (Engel et al., 1997), a net imaging force of 25 pN and an average surface charge density of the AFM probe of -0.032 C/m^2 (Butt, 1991) we calculate an electrostatic field of 6.19×10^7 V/m from the AFM data (using Coulomb's law). At a monovalent electrolyte concentration of 100 mM KCl this field strength was reached at a pore depth of 0.5 nm below the periplasmic bilayer surface, whereas at 50 mM KCl the same field strength was reached at a pore depth of 0.3 nm.

Simulating the experiment

Two facts are known from the AFM experiment: the constant force mode operates at ~25 pN and the observed height difference between the topographs recorded at 50 mM salt and 300 mM salt concentrations is 0.5 nm. In an attempt to reproduce these values theoretically, the electrostatic potential and the resulting forces were calculated by two different approaches. These were based on similar settings, such as using the same atomic coordinates, radii, and charges (for details, see Materials and Methods). The two approaches differed markedly in their treatment of the AFM probe. Approach A did not include the probe at all during the solution of the PB equation but only a posteriori by using a point charge of -2.51 e in the force calculation. Approach B, however, included the probe as a low-dielectric, ion-excluding sphere into the PB equation, solving the system for every given probe position. Whereas approach A only requires a single solution of the PB equation, the resulting force cannot correlate the experimental forces with the measured height difference, as displayed in Fig. 4: The isoforce surface at -25 pN is marginally different for the two ion concentrations, whereas the height difference of 0.5 nm can only be obtained by a contour of ~ -5 pN. The calculated force is thus significantly smaller than the applied external force and hence Approach A gives a qualitative picture of the electrostatic potential only. By modeling the probe as a sphere of 1-nm radius, and including it into the PB equation in terms of its dielectric constant, its exclusion of mobile counterions, and its surface charge, Approach B can overcome this discrepancy. However, the PB equation must be solved and the electrostatic interaction energy G_{elec} between probe and OmpF porin derived for every given position of the probe (as explained in Materials and Methods, Approach B). As presented in Fig. 5, the results of this approach are in quantitative agreement with the experimental measurements. In contrast, the total microscopic force is smaller than 10 pN if the physical probe is not explicitly included in the calculations (the results are shown only for 50 mM salt concentration yielding the largest force), which is exactly what was observed for Approach A. When the physical probe is not included explicitly, the average microscopic force is simply given by qE, in which q represents the charge of the probe and E the electrostatic field generated by OmpF. But this expression neglects the forces arising from the presence of the low dielectric of the probe near OmpF (Im and Roux, 1998). In fact, it can be shown that there is a dielectric repulsion even if the probe does not carry any charge.

The calculations demonstrate that it is essential to include the AFM probe explicitly to reach a quantitative agreement with the measured displacements as a function of salt con-

centration. The agreement between the calculations and the measured displacements is remarkable and suggests that a quantitative interpretation of electrostatic maps recorded by AFM may be possible. This opens the avenue to the direct measurement of electrostatic fields at the molecular level.

CONCLUSION

AFM can be used to contour surface structure and to probe electrostatic potential of a native membrane protein at a resolution < 1 nm. Experimental data and calculations show OmpF porin to generate an asymmetric electrostatic potential, which increases with decreasing electrolyte concentration. The calculations based on the numerical solution to the PB equation show that this potential arises from the charges lining the center of the transmembrane pore. Both results suggest that the previously detected ion selectivity of OmpF finds its origin by this electrical potential produced by the protein. However, whether the observed asymmetry of the potential is of functional importance remains to be answered. In future the combination of AFM and theoretical calculations may be applied to learn about the structure function relationship of other ion selective channels. The calculations demonstrate unambiguously that the amount of electrostatic forces is also determined by local interaction between AFM probe and the protein. Most interestingly, the method introduced here is applicable to membrane proteins as well as to water-soluble proteins and will allow detecting and localizing changes in their electrostatic potential.

We thank M. Cyrklaff and A. Hoenger for providing the OmpF porin crystals and are grateful to R. Dutzler, J. Howard, S. A. Müller, and B. Sakmann for stimulating discussions. The Swiss National and the M. E. Müller foundation supported this work.

REFERENCES

Binnig, G., C. F. Quate, and C. Gerber. 1986. Atomic force microscope. *Phys. Rev. Lett.* 56:930–933.

Butt, H-J. 1991. Measuring electrostatic, van der Waals, and hydration forces in electrolyte solutions with an atomic force microscope. *Biophys. J.* 60:1438–1444.

Butt, H-J., M. Jaschke, and W. Ducker. 1995. Measuring surface forces in aqueous solution with the atomic force microscope. *Bioelect. Bioenerg.* 38:191–201.

Cowan, S. W., T. Schirmer, G. Rummel, M. Steiert, R. Ghosh, R. A. Pauptit, J. N. Jansonius, and J. P. Rosenbusch. 1992. Crystal structures explain functional properties of two *E. coli* porins. *Nature.* 358:727–733.

Czajkowsky, D. M., H. Iwamoto, T. L. Cover, and Z. Shao. 1999. The vacuolating toxin from *Helicobacter pylori* forms hexameric pores in lipid bilayers at low pH. *Proc. Natl. Acad. Sci. U.S.A.* 96:2001–2006.

Drake, B., C. B. Prater, A. L. Weisenhorn, S. A. C. Gould, T. R. Albrecht, C. F. Quate, D. S. Cannell, H. G. Hansma, and P. K. Hansma. 1989. Imaging crystals, polymers, and processes in water with the atomic force microscope. *Science.* 243:1586–1588.

Ducker, W. A., T. J. Senden, and R. M. Pashley. 1991. Direct measurements of colloidal forces using an atomic force microscope. *Nature.* 353:239–241.

Dutzler, R., G. Rummel, S. Alberti, S. Hernandez-Alles, P. Phale, J. Rosenbusch, V. Benedi, and T. Schirmer. 1999. Crystal structure and functional characterization of OmpK36, the osmoporin of *Klebsiella pneumoniae*. *Struct. Fold. Des.* 7:425–434.

Engel, A., and D. J. Müller. 2000. Observing single biomolecules at work with the atomic force microscope. *Nat. Struct. Biol.* 7:715–718.

Engel, A., C-A. Schoenenberger, and D. J. Müller. 1997. High-resolution imaging of native biological sample surfaces using scanning probe microscopy. *Curr. Opin. Struct. Biol.* 7:279–284.

Heinz, W. F., and J. H. Hoh. 1999. Relative surface charge density mapping with the atomic force microscope. *Biophys. J.* 76:528–538.

Hoenger, A., R. Ghosh, C-A. Schoenenberger, U. Aebi, and A. Engel. 1993. Direct in situ structural analysis of recombinant outer membrane proteins expressed in an OmpA-deficient mutant *Escherichia coli* strain. *J. Struct. Biol.* 111:212–221.

Hoenger, A., H. Gross, A. Engel. 1990. Localization of the lipopolysaccharides in metal-shadowed reconstituted lipid-porin membranes. *J. Struct. Biol.* 103:185–195.

Honig, B., and A. Nicholls. 1995. Classical electrostatics in biology and chemistry. *Science.* 268:1144–1149.

Im, W., and B. Roux. 1998. Continuum solvation model: electrostatic forces from numerical solutions to the Poisson-Boltzmann equation. *Comp. Phys. Commun.* 111:59–75.

Im, W., S. Seefeld, and B. Roux. 2000. Grand canonical Monte Carlo-Brownian dynamics algorythm for simulating ion channels. *Biophys. J.* 79:788–801.

Israelachvili, J. 1991. Intermolecular and surface forces. Academic Press Limited, London.

Karshikoff, A., V. Spassov, S. W. Cowan, R. Ladenstein, and T. Schirmer. 1994. Electrostatic properties of two porin channels from *Escherichia coli*. *J. Mol. Biol.* 240:372–384.

Kirkwood, J. G. 1934. Theory of solution of molecules containing widely separated charges with application to zwiterions. *J. Chem. Phys.* 2:351.

Klebba, P. E., and S. M. Newton. 1998. Mechanisms of solute transport through outer membrane porins: burning down the house. *Curr. Opin. Microbiol.* 1:238–247.

Lou, K-L., N. Saint, A. Prilipov, G. Rummel, S. A. Benson, J. P. Rosenbusch, and T. Schirmer. 1996. Structural and functional characterization of OmpF porin mutants selected for larger pore size. *J. Biol. Chem.* 271:20669–20675.

MacKerell, A. D., D. Bashford, M. Bellot, R. L. Dunbrack, J. D. Evanseck, M. J. Field, S. Fischer, J. Gao, H. Guo, D. Joseph-McCarthy, et al. 1998. All-atom empirical potential for molecular modeling and dynamics studies of proteins. *J. Phys. Chem. B.* 102:3586–3616.

Madura, J. D., J.M. Briggs, R. C. Wade, M. E. Davies, B. A. Luty, A. Ilin, J. Antosiewicz, M. K. Gilson, B. Bagheri, L. R. Scott, et al. 1995. Electrostatics and diffusion in solution: simulations with the University of Houston Brownian Dynamics Program. *Comp. Phys. Commun.* 91: 57–95.

McLaughlin, S. 1989. The electrostatic properties of membranes. *Annu. Rev. Biophys. Chem.* 18:113–136.

Müller, D. J., M. Amrein, and A. Engel. 1997. Adsorption of biological molecules to a solid support for scanning probe microscopy. *J. Struct. Biol.* 119:172–188.

Müller, D. J., and A. Engel. 1997. The height of biomolecules measured with the atomic force microscope depends on electrostatic interactions. *Biophys. J.* 73:1633–1644.

Müller, D. J., D. Fotiadis, and A. Engel. 1998. Mapping flexible protein domains at subnanometer resolution with the AFM. *FEBS Lett.* 430: 105–111.

Müller, D. J., D. Fotiadis, S. Scheuring, S. A. Müller, and A. Engel. 1999. Electrostatically balanced subnanometer imaging of biological specimens by atomic force microscopy. *Biophys. J.* 76:1101–1111.

Nakamara, H. 1996. Roles of electrostatic interaction in proteins. *Q. Rev. Biophys.* 29:1–90.

Nikaido, H., and M. H. Saier. 1992. Transport proteins in bacteria: common themes in their design. *Science.* 258:936–942.

Nina, M., D. Beglov, and B. Roux. 1997. Atomic radii for continuum electrostatics calculations based on molecular dynamics free energy simulations. *J. Phys. Chem. B.* 101:5239–5248.

Pashley, R. M. 1981. Hydration forces between mica surfaces in Li^+, Na^+, Na^+ and Cs^+ electrolyte solutions: a correlation of double layer and hydration forces with surface cation exchange properties. *J. Colloid Interface Sci.* 83:531–546.

Rotsch, C., and M. Radmacher. 1997. Mapping local electrostatic forces with the atomic force microscope. *Langmuir.* 13:2825–2832.

Roux, B., S. Berneche, and W. Im. 2000. Ion channels, permeation, and electrostatics: insight into the function of KcsA. *Biochemistry.* 39: 13295–13306.

Roux, B., and R. MacKinnon. 1999. The cavity and pore helices in the KcsA K+ channel: electrostatic stabilization of monovalent cations. *Science.* 285:100–102.

Roux, B., and T. Simonson. 1999. Implicit solvent models. *Biophys. Chem.* 78:1–20.

Saint, N., K. L. Lou, C. Widmer, M. Luckey, T. Schirmer, and J. P. Rosenbusch. 1996a. Structural and functional characterization of OmpF porin mutants selected for larger pore size. *J. Biol. Chem.* 271: 20676–20680.

Saint, N., A. Prilipov, A. Hardmeyer, K-L. Lou, T. Schirmer, and J. P. Rosenbusch. 1996b. Replacement of the sole histidinyl residue in OmpF porin from *E. coli* by theronine (H21T) does not affect channel structure and function. *Biochem. Biophys. Res. Commun.* 223:118–122.

Sanner, M. F., A. J. Olson, and J. C. Spehner. 1996. Reduced surface: an efficient way to compute molecular surfaces. *Biopolymers*. 38:305–320.

Schabert, F. A., and A. Engel. 1994. Reproducible acquisition of *Escherichia coli* porin surface topographs by atomic force microscopy. *Biophys. J.* 67:2394–2403.

Schabert, F. A., C. Henn, and A. Engel. 1995. Native *Escherichia coli* OmpF porin surfaces probed by atomic force microscopy. *Science.* 268:92–94.

Schirmer, T. 1998. General and specific porins from bacterial outer membranes. *J. Stuct. Biol.* 121:101–109.

Schirmer, T., and P. S. Phale. 1999. Brownian dynamics simulation of ion flow through porin channels. *J. Mol. Biol.* 294:1159–1167.

Sharp, K. A., and B. Honig. 1990. Electrostatic interactions in macromolecules: theory and application. *Annu. Rev. Biophys. Chem.* 19:301–332.

Weisenhorn, A. L., M. Khorsandi, S. Kasas, V. Gotzos, and H-J. Butt. 1993. Deformation and height anomaly of soft surfaces studied with an AFM. *Nanotechnology.* 4:106–113.

Weiss, M. S., U. Abele, J. Weckesser, W. Welte, E. Schlitz, and G. E. Schulz. 1991. Molecular architecture and electrostatic properties of a bacterial porin. *Science.* 254:1627–1630.